

Article

Benefits of Intelligent Fuzzy Controllers in Comparison to Classical Methods for Adaptive Optics

Victor Costa [†]  and Wesley Beccaro ^{*,†} 

Department of Electronic Systems Engineering, Polytechnic School, University of São Paulo, São Paulo 05508-010, Brazil; costa.victor@usp.br

* Correspondence: wesley@lme.usp.br

[†] These authors contributed equally to this work.

Abstract: Adaptive Optics (AO) systems have been developed throughout recent decades as a strategy to compensate for the effects of atmospheric turbulence, primarily caused by poor astronomical seeing. These systems reduce the wavefront distortions using deformable mirrors. Several AO simulation tools have been developed, such as the Object-Oriented, MATLAB, and Adaptive Optics Toolbox (OOMAO), to assist in the project of AO. However, the main AO simulators focus on AO models, not prioritizing the different control techniques. Moreover, the commonly applied control strategies in ground-based telescopes are based on Integral (I) or Proportional-Integral (PI) controllers. This work proposes the integration of OOMAO models to Simulink to support the development of advanced controllers and compares traditional controllers with intelligent systems based on fuzzy logic. The controllers were compared in three scenarios of different turbulence and atmosphere conditions. The simulations were performed using the characteristics/parameters of the Southern Astrophysical Research (SOAR) telescope and assessed with the Full Width at Half Maximum (FWHM), Half Light Radius (HLR), and Strehl ratio metrics to compare the performance of the controllers. The results demonstrate that adaptive optics can be satisfactorily simulated in OOMAO adapted to Simulink and thus further increase the number of control strategies available to OOMAO. The comparative results between the MATLAB script and the Simulink blocks designed showed a maximum relative error of 3% in the Strehl ratio and 1.59% in the FWHM measurement. In the assessment of the control algorithms, the fuzzy PI controller reported a 25% increase in the FWHM metrics in the critical scenario when compared with open-loop metrics. Furthermore, the fuzzy PI controller outperformed the results when compared with the I and PI controllers. The findings underscore the constraints of conventional control methods, whereas the implementation of fuzzy-based controllers showcases the promise of intelligent approaches in enhancing control performance under challenging atmospheric conditions.

Keywords: adaptive optics; intelligent controllers; instrumentation; simulation; wavefront sensors; point-spread functions



Citation: Costa, V.; Beccaro, W. Benefits of Intelligent Fuzzy Controllers in Comparison to Classical Methods for Adaptive Optics. *Photonics* **2023**, *10*, 988. <https://doi.org/10.3390/photonics10090988>

Received: 15 June 2023

Revised: 13 August 2023

Accepted: 28 August 2023

Published: 30 August 2023



Copyright: © 2023 by the authors. Licensee MDPI, Basel, Switzerland. This article is an open access article distributed under the terms and conditions of the Creative Commons Attribution (CC BY) license (<https://creativecommons.org/licenses/by/4.0/>).

1. Introduction

Telescopes are instruments designed to observe distant celestial bodies. Normally, a few photons from these bodies reach the instrument, which requires the development of an infrastructure for capturing and correcting noise and distortions [1–5].

Atmospheric turbulence is a key factor in the degradation of the image obtained by ground-based optical telescopes. This phenomenon, called seeing, limits the resolution of these instruments. Since the 1950s, AO techniques have been used to mitigate this effect [6]. Atmospheric turbulence can be compensated by geometric modifications of deformable mirrors employing real-time systems and wavefront sensors [7–14].

Typically, the final technology employed to implement AO systems in telescopes demands the use of numerical simulations before the direct integration of the control systems [15]. To support the design of AO systems, several models of atmospheric turbulence

and astronomical instruments have been developed over the years. YAO, developed in Yorick, is a classic implementation of AO simulation [16]. Currently, other simulators have shown excellent results, such as Simulation ‘Optique Adaptative’ with Python (SOAPY) [17], AOtools [18], both developed in Python, and the Object-Oriented, MATLAB and Adaptive Optics Toolbox (OOMAO), which is developed in MATLAB® [19]. OOMAO is a toolbox dedicated to AO systems that uses the object-oriented paradigm and features an atmospheric turbulence generation model proposed by [20]. Since it is numerically more efficient than traditional Monte Carlo models, it allows the simulation of atmospheric turbulence effects on larger telescopes. The OOMAO framework also implements models of source, atmosphere, telescope, wavefront sensor (Shack–Hartmann), and deformable mirror.

OOMAO mainly focuses on adaptive optics models, not prioritizing the different control strategies. Although it is possible to implement alternative strategies, there is a difficulty in adapting control techniques other than those already implemented in the toolbox (i.e., integral controller using the reconstruction obtained from Singular Value Decomposition (SVD), open-loop controller, and modal controller). One way to overcome this limitation is integrating OOMAO with Simulink—MathWorks software focusing on modeling, simulation, and analysis of dynamic systems—which enables the designer to focus on the controller project at a high level of abstraction and maintaining AO models encapsulated in blocks. By employing this approach, it becomes possible to assess the performance enhancements of AO systems by evaluating various control strategies, such as intelligent controllers [21]. It is worth emphasizing that this integration is not a straightforward task. First, it requires the reconfiguration of functions and operations carried out during simulations. Second, despite Simulink being a specialized tool within MATLAB, it can employ a different set of solvers and methods for dynamical simulation. To ensure proper functionality, it is necessary to validate the integration of MATLAB functions in Simulink. This verification confirms the seamless interaction between MATLAB functions and Simulink, ensuring that the desired behavior of the control system is achieved as intended.

This work proposes the integration of the models developed in OOMAO into Simulink and compares classical and intelligent control techniques for adaptive optics. A comparative analysis between the open-loop system and closed-loop systems implemented with Integral (I), Proportional-Integral (PI), and Fuzzy-based controllers is presented. The main contributions of the paper can be summarized as follows:

- The integration and evaluation of OOMAO models into Simulink.
- As proof of concept, intelligent controllers have been developed and compared with traditional ones, illustrating how to assess controllers in scenarios with different turbulence and atmospheric conditions using performance metrics commonly employed in AO projects.
- We have demonstrated the potential of fuzzy logic controllers over conventional controllers in the AO design, reporting some advantages of the intelligent approach such as the wider range of operating conditions, the capacity to include the experience in the controller rules, and the better performance when compared with conventional controllers.

The remainder of the article is organized as follows: Section 2 briefly presents an overview of classical and hybrid fuzzy logic controllers. Section 3 describes the simulation parameters, the adaptive optics quality metrics, and the scenarios considered for the simulations. Section 4 presents the results and discussions of the integration of OOMAO with Simulink and the comparative evaluation of the controllers. Finally, Section 5 describes the conclusion.

2. Overview of Classical and Intelligent Controllers

2.1. PID Controllers

PID controllers are applied to most modern process control systems today [22]. The parallel PID algorithm is described as

$$u(t) = K_p \left[e(t) + \frac{1}{T_i} \int_0^t e(\tau) d\tau + T_d \frac{de(t)}{dt} \right], \quad (1)$$

where $e(t)$ and $u(t)$ are, respectively, the control error ($e(t) = r(t) - y(t)$, reference set point minus the measured process variable) and the control signal. K_p is the proportional gain, T_i is the integral time, and T_d is the derivative time. Another way to express the PID is in terms of K_p , $K_i = K_p/T_i$, and $K_d = K_p T_d$, respectively, proportional, integral, and derivative gains.

The digital implementation of the PID requires discretizing the integral and derivative actions using approximations (e.g., forward, backward, or trapezoidal approximations). It is possible to discretize the integral action separately from the derivative action. To avoid sharp changes in integral action when sudden changes occur in setpoint or process variable signals, the trapezoidal integration (also known as Tustin or Bilinear transformation) can be applied to the integral action, obtaining

$$u_I(k+1) = u_I(k) + \frac{K_p T_s}{T_i} \left[\frac{e(k+1) + e(k)}{2} \right], \quad (2)$$

where T_s is the sampling time and k is the discrete time [23]. The I-part can be precalculated right after the PID calculation. The derivative action is usually discretized by the backward approximation technique [23], which results in the expression

$$u_D(k) = \frac{T_d}{T_d + NT_s} u_D(k-1) - \frac{K_p T_d N}{T_d + NT_s} [y(k) - y(k-1)], \quad (3)$$

considering the ideal derivative action filtered by a first-order system with the time constant T_d/N (often N is between 8 and 20), which acts as a low-pass filter, limiting the high-frequency measurement noise. Alternatively, $u_D(k) = \frac{K_p T_d}{T_s} [e(k) - e(k-1)]$ in its most basic form.

The proportional term is implemented by replacing the continuous variables with their sampled versions as $u_P(k) = K_p e(k)$ and the control signal is given by $u(k) = u_P(k) + u_I(k) + u_D(k)$.

Normally, when designing a PID controller, the dynamics of the sensors and actuators are taken into account to determine the response and accommodation times of the closed-loop system. However, in some cases, such as the deformable mirror described by OOMAO, considering the sampling rates normally used in AO systems, the dynamics are fast enough for its accommodation to be considered instantaneous.

2.2. Fuzzy Based Controllers

The PID controller, due to its robustness and simplicity, is widely employed in the industry; however, the algorithm has low performance when applied to non-linear systems. An alternative to PID that introduces nonlinearities to the controller is the incorporation of fuzzy logic strategies. Fuzzy controllers formalize human reasoning in control systems. In general, they are composed of three blocks: fuzzification, fuzzy inference engine, and defuzzification.

The fuzzification changes the input variables into a fuzzy value using different membership functions typically built with sine, trapezoid, and triangle functions. The expert-defined fuzzy rules, commonly expressed as “if-then” statements, are integrated into the fuzzy inference engine. The inference procedure utilizes this knowledge base to determine a reasonable output based on linguistic terms. Finally, the defuzzification converts the output into a crisp value, in the case of the hybrid fuzzy PID controller, the K_p , T_i , and T_d

parameters, for example. Various defuzzification methods, including the center of mass, the center of area, minimum and maximum, and others, can be employed for this purpose [24].

We have proposed a hybrid fuzzy PI architecture, as presented in Figure 1, since it incorporates the fuzzy inference system as a supervisor of the PI controller. The determination of the parameters of the controller (i.e., proportional gain and integral time) relies on the fuzzy logic, employing linguistic parameters and the Mamdani fuzzy inference system.

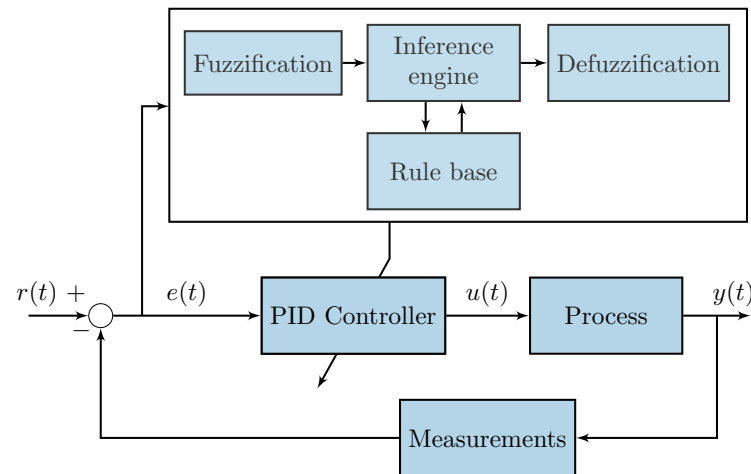


Figure 1. Hybrid Fuzzy PID control block diagram. In detail, the steps of fuzzy reasoning comprise the fuzzification, inference engine, and defuzzification blocks.

2.3. Intelligent Adaptive Optics

There exist some innovative proposals that involve the integration of intelligent techniques, including fuzzy logic, machine learning, and other intelligent algorithms in the context of AO. These strategies aim to enhance the capabilities of AO systems by leveraging intelligent approaches to address the challenges posed by atmospheric turbulence and wavefront distortions.

Within the framework of fuzzy controllers, Ke and Zhang [25] employed a fuzzy control algorithm to adjust the parameters of the PID controller within the deflection mirror loop. Florez-Meza et al. [26] presented a study that focused on the application of fuzzy control in the AO tip-tilt system. The authors demonstrated the effectiveness of the fuzzy approach, showcasing high stability and robustness indices. Regarding machine learning methods, Nousiainen et al. [21] put forth the concept of modeling a closed-loop AO system as a Markov decision process (MDP). They conducted an evaluation of the performance of conventional deep reinforcement learning algorithms on the AO system, considering a telescope diameter equal to 8 m. A similar control strategy was implemented in [27]. Pou et al. [28] introduce a control algorithm based on multi-agent reinforcement learning (MARL). This approach allows the controller to learn a non-linear policy without requiring prior knowledge of atmospheric dynamics. The results obtained, conducted on an 8 m telescope with a 40×40 WFS, demonstrate a performance improvement compared to the integrator baseline. Furthermore, the performance achieved by the MARL-based approach is comparable to a model-based predictive strategy that utilizes a linear quadratic Gaussian controller and has prior knowledge of atmospheric conditions. Guo et al. [29] conducted a comprehensive review of AO focusing on machine learning algorithms. The authors examined the blocks that constitute the AO systems and explored the potential integration of machine learning algorithms into each of these parts.

3. Materials and Methods

Figure 2 illustrates the flow diagram adopted for analyzing the controllers. The AO control loop simulation requires configuring the various parameters of the models, such as

the simulation scenarios, which describe general atmospheric conditions, the turbulence intensity, the light source, the telescope characteristics, and the control metrics adopted.

Three distinct simulation scenarios were adopted: typical, worst, and critical cases. They are based on nominal atmospheric conditions observed at the SOAR telescope site, situated at an elevation of 2738 m in Cerro-Pachón, Chile. The SOAR telescope has been designed to operate across a broad spectral range, from the atmospheric cut-off in the blue wavelength (320 nm) to the near-infrared. Simulation scenarios and adaptive optics metrics are described in Sections 3.2 and 3.3.

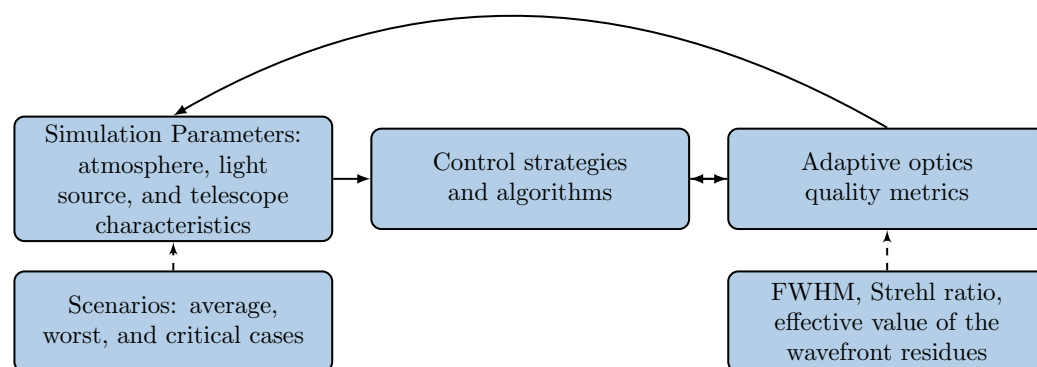


Figure 2. Flow diagram for testing and validating AO controllers simulations.

As mentioned previously, we have applied I, PI, and fuzzy PI controllers instead of PID and fuzzy PID controllers (i.e., disregarding the derivative action). In general, PI and fuzzy PI controllers are more adequate to reduce the steady-state error than their PID versions.

3.1. Simulation Parameters: Atmosphere, Light Source, and Telescope Characteristics

Prior to any simulation in OOMAO, it is essential to create and define certain simulation classes such as light source, atmosphere, telescope, Shack–Hartmann wavefront sensor (WFS), and deformable mirror. Those objects are instantiated by calling their constructors and aggregated through overloaded operators [30].

Considering the atmospheric and instrumentation information extracted from the SOAR telescope, an object from the telescope class was created with the diameter of the primary mirror, D , equal to 4.1 m and field of view of 3×3 arcmin, according to the SOAR adaptive optics module (SAM) and its upgraded counterpart, SAMplus. SAM was developed to compensate for the effects of ground-layer atmospheric turbulence across a wide range of wavelengths, including near-infrared (IR) and visible wavelengths [8]. It was initially developed utilizing the bimorph DM technology, featuring 60 actuators. SAM incorporated a Shack–Hartmann WFS with a 10×10 configuration, utilizing an 80×80 pixel CCD-39. SAMplus represents an upgraded iteration of the SAM that features an increased number of DM and WFS.

The laser guide star (LGS) was projected at an altitude of 7062 m in the U band. The second source simulates, in the I band, the star to be corrected, positioned at infinity. The Shack–Hartmann WFS was instantiated with 16×16 lenslets, with each lenslet consisting of 8×8 pixels. A deformable mirror was created with 17×17 actuators. Both the WFS and the deformable mirror actuators are arranged in square grids. Additionally, a camera with dimensions of 128×128 pixels was utilized. Moreover, in the description of the telescope class, the central obscuration ratio was established at 0.228 (22.8%). The influence of spider structures has been disregarded.

The atmospheric data consists of different scenarios simulating atmospheric turbulence ranging from a typical case to a critical case. The Fried parameter, r_0 , ranges from 10 to 14 cm while the wind speed goes from 9 to 40 m/s. The simulations were performed at the I band (approximately 790 nm). The stellar magnitude was set to 3.3.

3.2. Adaptive Optics Quality Metrics

In general, the goal of an AO control loop is to minimize the residual phase of the measured wavefront. Several techniques measure the quality of an adaptive optics control loop, depending on the type of astronomical observation one intends to perform. Among the metrics, this report employs the following methods to analyze and compare the outcomes of various AO control strategies put forth: FWHM of the point-spread function (PSF), which is the diffraction pattern formed by the wavefront; the Strehl ratio, measuring the effective value of the wavefront residues; and the HLR [31]. In the conducted simulations, the Strehl ratio is represented in percentage form. Those metrics were chosen once they represent a mix between metrics commonly used in AO (i.e., FWHM and Strehl ratio) and control metrics that are more readily obtainable in real time (e.g., the effective value from wavefront residues). Specifically, the FWHM was estimated by taking the average of the FWHM values computed in the xz - and yz -plane, corresponding to the x - and y -axis, respectively.

3.3. Simulation Scenarios

As shown in Figure 2, three simulation scenarios were established. In each scenario, five atmospheric layers were created at altitudes ranging from 0 to 8 km. Each atmospheric layer represents different partial contributions to the atmospheric turbulence and wind velocity, following the same criterion established in simulations for the SAMplus [8]. The way in which these parameters were grouped is described in Table 1. The wind speed in each atmospheric turbulence layer was also grouped into typical, worst, and critical cases. In the typical case, winds of at most 25 m/s were considered while the winds reach 40 m/s in the critical case. Table 2 presents a description of the wind speeds simulated in each scenario.

Table 1. Indication of r_0 and total contribution of each atmospheric layer in the seeing phenomenon. Considering the typical case (I), the worst case (II), and the critical case (III) [8].

Layer	1	2	3	4	5	R_0 [cm]
Altitude [km]	0	1	2	4	8	-
Fractional r_0 —I	0.74	0.02	0.02	0.10	0.12	14
Fractional r_0 —II	0.70	0.03	0.07	0.10	0.10	11
Fractional r_0 —III	0.65	0.05	0.09	0.11	0.10	10

Table 2. Wind speed in each atmospheric layer, considering the typical case (I), the worst case (II), and the critical case (III) [8].

Layer	1	2	3	4	5
Altitude [km]	0	1	2	4	8
Wind speed—I	9 m/s	10 m/s	15 m/s	25 m/s	25 m/s
Wind speed—II	15 m/s	25 m/s	25 m/s	30 m/s	35 m/s
Wind speed—III	25 m/s	25 m/s	30 m/s	35 m/s	40 m/s

4. Results and Discussion

4.1. Integration of OOMAO with Simulink

As above mentioned, OOMAO is focused on AO modeling strategies, while Simulink has a standard library with many available controllers and is fully integrated with MATLAB. To speed up the process of simulating non-native controllers (e.g., fuzzy-based controllers) in OOMAO, an adaptation layer between OOMAO and Simulink was developed. Figure 3 presents an example of a block diagram implemented using the adapted OOMAO blocks in Simulink. To showcase the capabilities of the integration, Figure 4a depicts the total incident wavefront, while Figure 4b,c illustrate the residual wavefront and the accumulated wavefront after the I controller action, respectively. Figure 4a exhibits a significant variation

in phase ranging from -20 to $40 \mu\text{m}$, which deviates from the ideal scenario as we desire values closer to zero. This is demonstrated in Figure 4b, which represents the controlled phase of the system. In addition to providing the capability to implement different control strategies, the integration also enhances the visualization of the results.

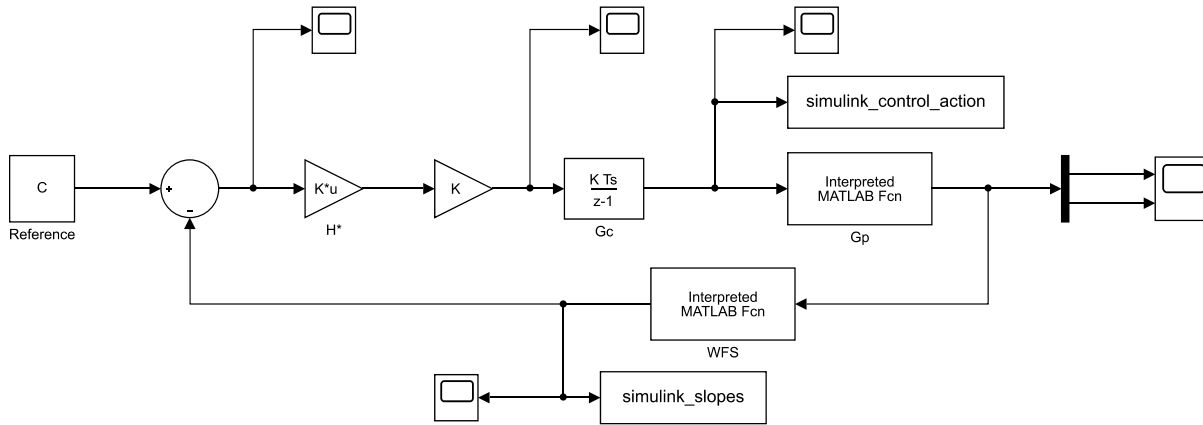


Figure 3. Block diagram of OOMAO simulation integrated with Simulink. G_c indicates the controller (in the example, a discrete-time Integral controller), G_p is the atmospheric turbulence process, H^* indicates the reconstruction matrix, and WFS the model of the Shack-Hartman wavefront sensor.

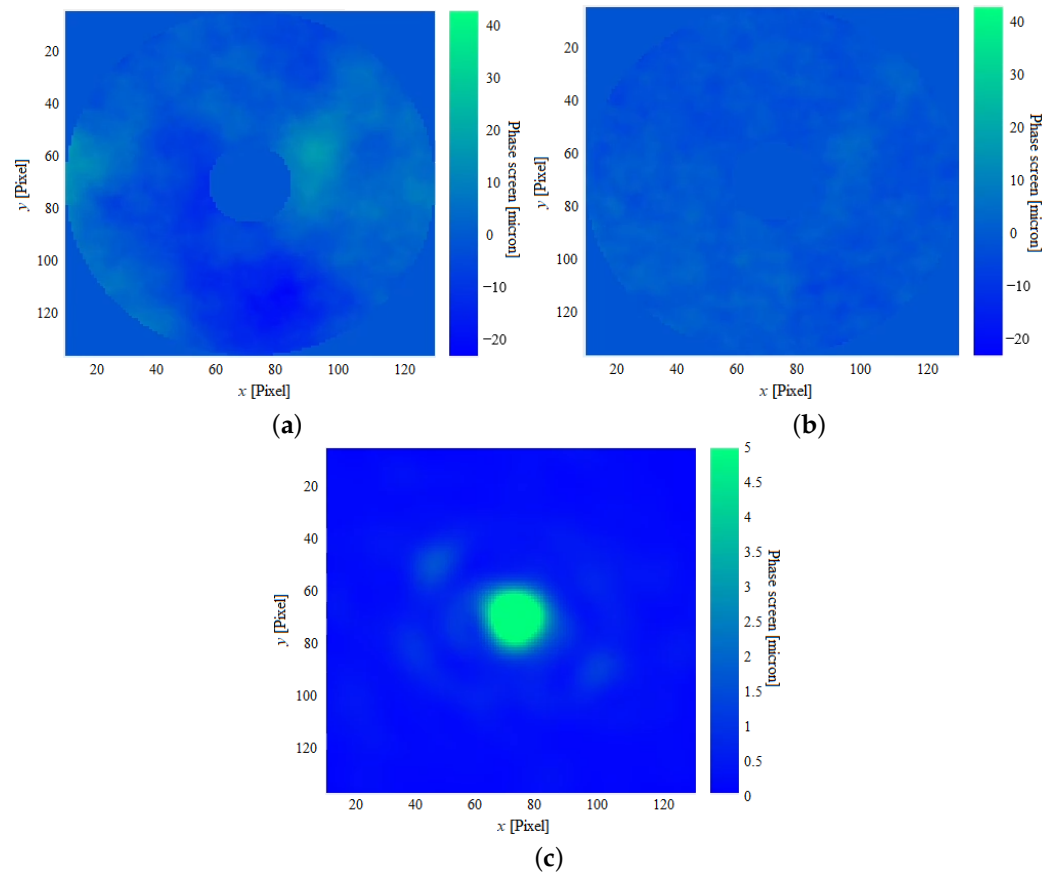


Figure 4. The total incident wavefront is represented in (a). The residual wavefront and the accumulated wavefront after the Integral controller action are indicated, respectively, in (b,c). The axes x and y represent the camera with 128×128 pixels and the z axis is the phase [μm].

Additionally, to validate this integration, the Integral controller was implemented, and the tests were replicated in both OOMAO and OOMAO integrated with Simulink. The

versions of the same controllers were compared under the conditions previously described in Section 3. The stochastic method used to simulate the atmospheric turbulence was fixed to the Mersenne twister using the seed identified as *mt19937ar* under the MathWorks environment. Figure 5 presents comparative graphs of wavefront RMS values versus time under the typical, worst, and critical cases, respectively. The results demonstrated a higher concordance between the curves obtained with the controller implemented in Simulink and with the native implementation of OOMAO in MATLAB, except for a short and constant 4-sample delay between the signal acquired from MATLAB and the one from Simulink. Simulink initiates from a starting point that is four steps ahead of the MATLAB code, as it executes the functions enclosed within the “Interpreted MATLAB Function” blocks multiple times. There is no need to include a delay block in Simulink, as the phase turbulence simulation yields valid results.

Table 3 compares the MSE of some variable computed between the implementation without (i.e., in the native code of OOMAO) and with the Simulink approach, here proposed.

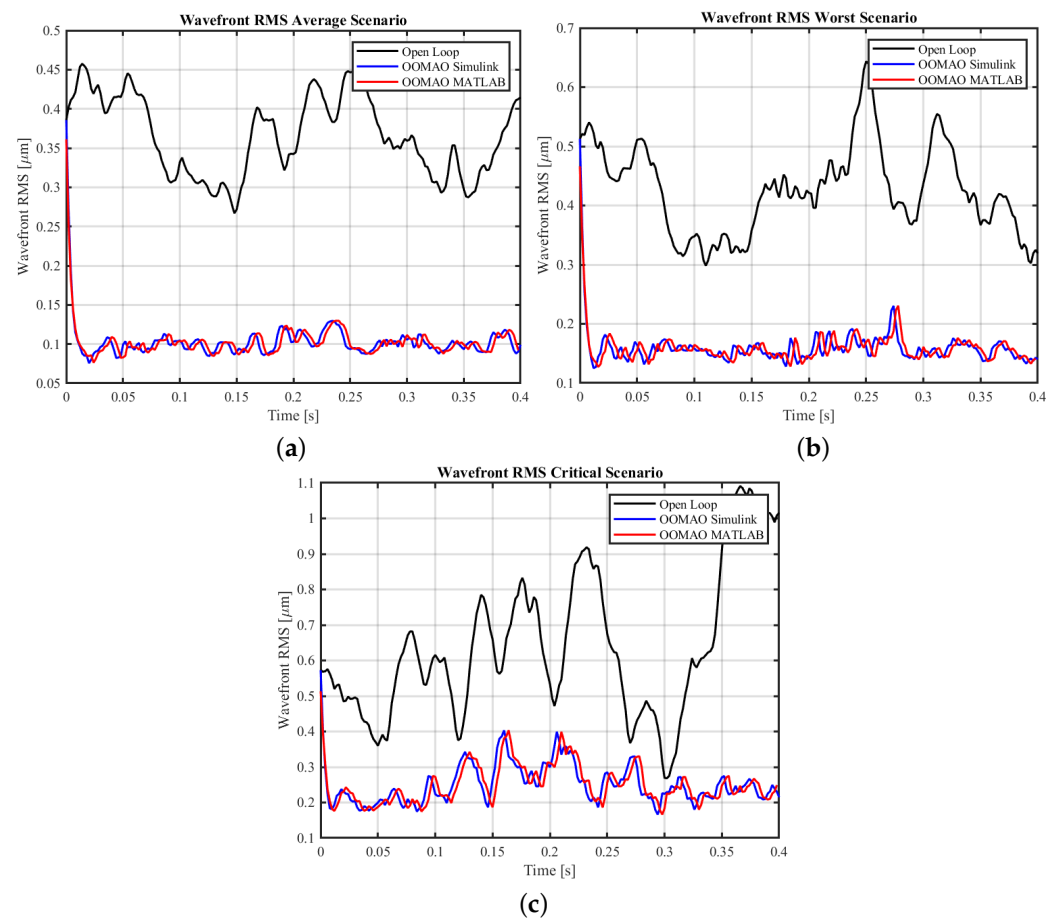


Figure 5. Wavefront RMS values over time for an open loop (black line), with the controller implemented in Simulink using the adaptation layer (blue line), and with the controller directly implemented in MATLAB without the adaptation layer (red line). Simulation scenarios: (a) typical case, (b) worst case, and (c) critical case. The delay between the curves of “OOMAO Simulink” and “OOMAO MATLAB” occurs due to internal processing aspects of the Simulink, not affecting the calculation.

Table 3. MSE of control variables calculated between implementation with and without the Simulink adaptation layer.

	Typical Scenario	Worst Scenario	Critical Scenario
MSE—Wavefront RMS values [μm^2]	7.49×10^{-5}	2.60×10^{-4}	9.82×10^{-4}
MSE—Slopes on first WFS lenslet [μm^2]	1.44×10^{-1}	7.17×10^{-1}	1.26×10^0
MSE—Slopes on last WFS lenslet [μm^2]	9.37×10^{-2}	2.93×10^{-1}	7.29×10^{-1}
MSE—DM first actuator control action amplitudes	3.11×10^{-16}	8.05×10^{-16}	1.09×10^{-15}
MSE—DM last actuator control action amplitudes	3.93×10^{-16}	6.95×10^{-16}	1.30×10^{-15}
MSE—DM control action RMS value amplitudes	1.18×10^{-17}	2.07×10^{-17}	5.41×10^{-17}

4.2. Numerical Simulation of Classical and Intelligent Controllers

4.2.1. Open-Loop Simulation

The open-loop simulations were carried out in each of the respective proposed scenarios. Figure 6a–c are the PSFs of the first open-loop turbulence profile in the typical, worst, and critical cases, respectively. The metrics of FWHM, HLR, and Strehl ratio in three turbulence profiles (T_1 , T_2 , and T_3) are shown in Table 4.

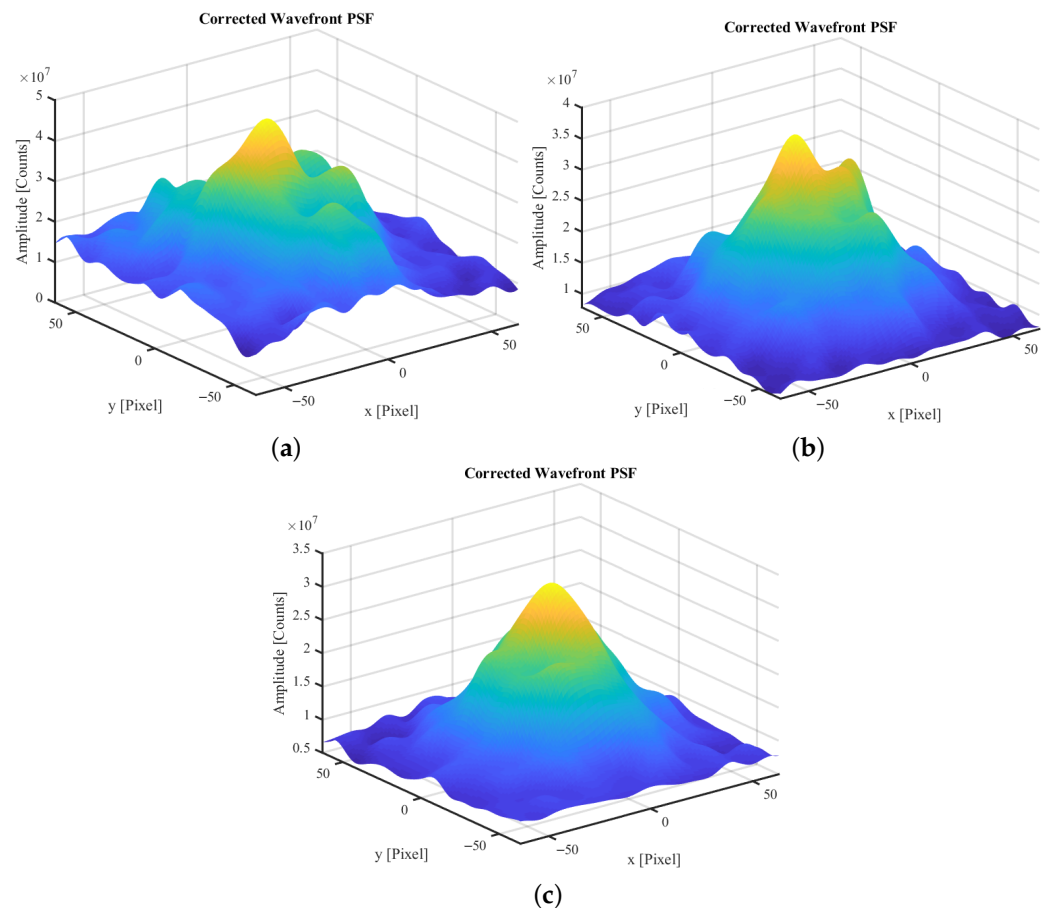


Figure 6. PSF of the first turbulence profile in an open loop for: (a) typical case, (b) worst case, and (c) critical case.

Comparing the results of the PSFs presented in Figure 6 with the value of an ideal PSF, it is possible to verify that the open-loop system is significantly noisier and less able to concentrate light when compared to the ideal one. One of the consequences of this fact is that the open-loop system does not have a PSF that is easily parameterized on a Gaussian or Moffat surface, which are more conventional surfaces for the characterization of PSF profiles [31]. Due to this difficulty, the proposed metrics may not be described effectively.

Therefore, not all metrics necessarily worsen due to atmospheric conditions; this implies that it is possible in some metrics of the open-loop system, the worst or the critical cases may have better indexes than the same metrics in the typical case, as is the case of FWHM and HLR. The Strehl ratio, which briefly indicates the ratio between the maximum points of the experimental PSF with the maximum point of the ideal PSF, can capture that the ability to concentrate energy worsens according to the atmospheric conditions.

Table 4. System performance in an open-loop for the cases analyzed in three turbulence profiles (T_1 , T_2 , and T_3) according to the metrics of FWHM [Pixel], HLR [Pixel], and Strehl ratio [%].

Metrics	Typical Scenario			Worst Scenario			Critical Scenario		
	T_1	T_2	T_3	T_1	T_2	T_3	T_1	T_2	T_3
FWHM	65.875	85	53.25	72.375	64.000	54.375	66.375	63.250	66.125
HLR	33.00	34.00	32.00	30.00	29.25	28.75	29.25	28.75	29.00
Strehl ratio	0.175%	0.184%	0.218%	0.124%	0.121%	0.157%	0.104%	0.110%	0.111%

4.2.2. Integral Controller

Figure 7a–c shows the PSFs of the first turbulence profile of the simulations of the I controller for the typical, worst, and critical scenarios, respectively. Table 5 presents a summary of the astronomical metrics evaluated. In the typical scenario, a reduction of the FWHM of around 40 pixels can be observed while no meaningful reduction was perceived either in the worst-case scenario or in the critical scenario. This conclusion can also be drawn by checking the PSF for each scenario, in which only the PSF of the typical case has a Gaussian-shaped surface with a high peak at the center and a symmetric bell-shaped surface.

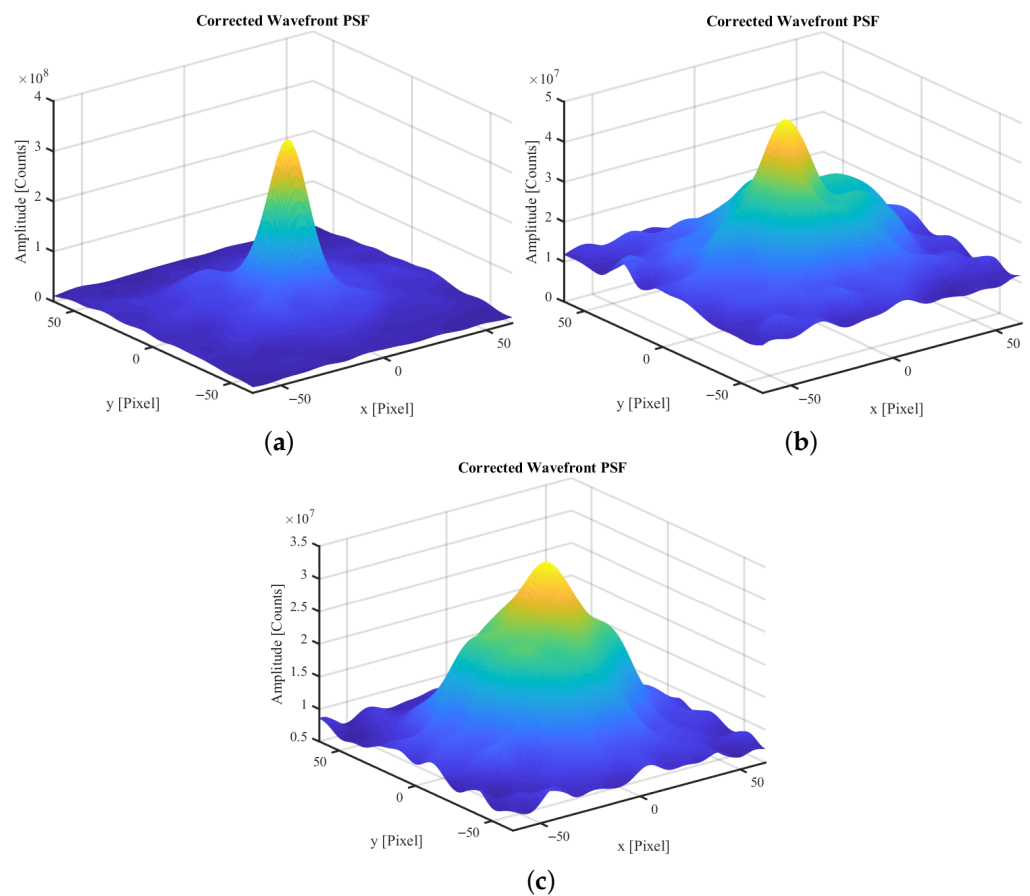


Figure 7. PSF of the first turbulence profile using an Integral action controller for: (a) typical case, (b) worst case, and (c) critical case.

In comparison with the metrics presented in Table 4, the I controller, in the typical case, performs significantly better than the open-loop system under the same conditions. This, however, is not necessarily true in the worst and most critical cases. Therefore, the I controller is sufficient to control the system only in good atmospheric conditions, since low-quality correction metrics were obtained in the worst and critical scenarios. Therefore, based on the results, conducting astronomical observations using AO (specifically, the I controller) on days with unfavorable atmospheric conditions would yield comparable results to systems without AO (i.e., open-loop).

Table 5. System performance with I controller for the cases analyzed in three turbulence profiles (T_1 , T_2 , and T_3) according to the metrics of FWHM [Pixel], HLR [Pixel], and Strehl ratio [%].

Metrics	Typical Scenario			Worst Scenario			Critical Scenario		
	T_1	T_2	T_3	T_1	T_2	T_3	T_1	T_2	T_3
FWHM	20.875	17.875	21.500	65.750	57.750	61.625	66.625	67.625	59.875
HLR	12.50	11.75	14.75	30.25	31.25	30.00	28.75	29.00	29.75
Strehl ratio	1.077%	1.303%	1.039%	0.162%	0.153%	0.129%	0.1097%	0.101%	0.113%

4.2.3. Proportional-Integral Controller

Figure 8a–c are the PSFs of the first turbulence profile controlled by the PI controller in the typical, worst, and critical cases, respectively. When comparing these PSFs with the ones obtained with the I controller, a greater concentration of energy is observed in all scenarios; moreover, the performance of the controller deteriorates significantly with the deterioration of the simulated atmospheric conditions.

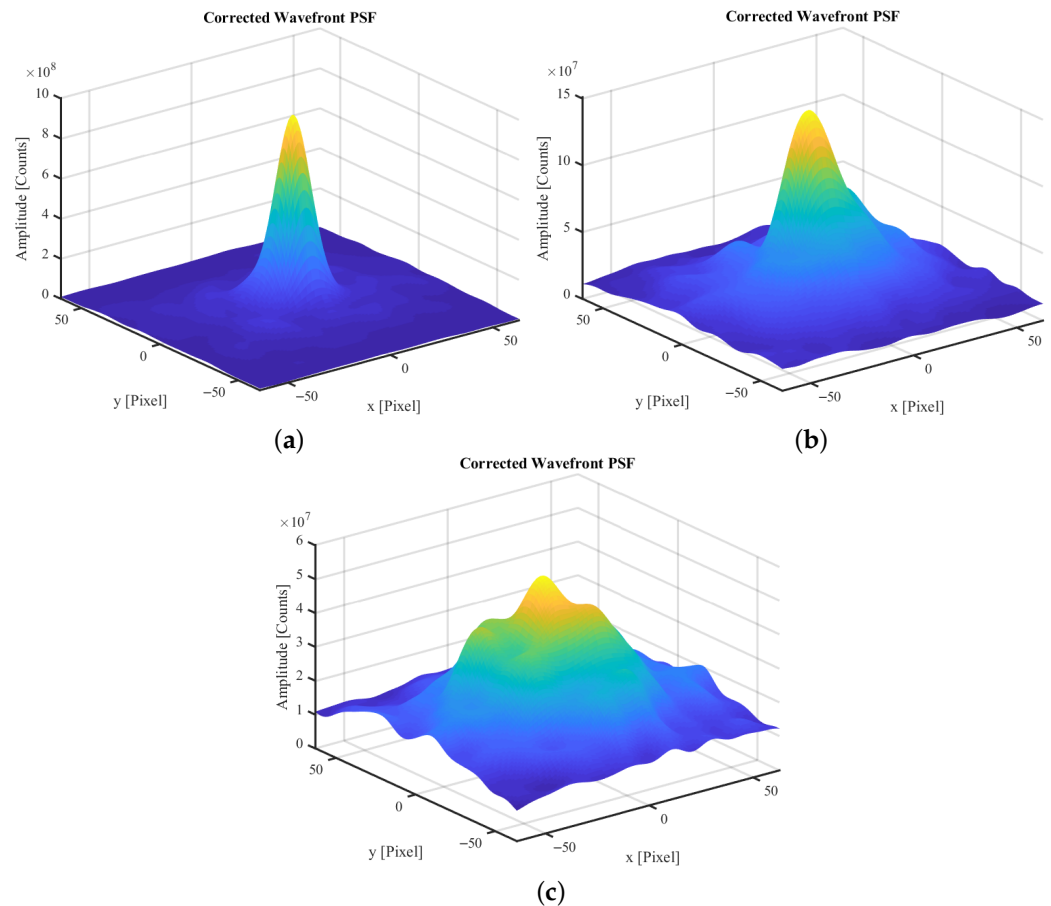


Figure 8. PSF of the first turbulence profile using PI action controller for: (a) typical case, (b) worst case, and (c) critical case.

The same conclusion can be reached by verifying the metrics in Table 6 with those provided in Tables 4 and 5, in which the metrics of FWHM and Strehl ratio obtained with the PI controller consistently performed better than the metrics of I controller and open-loop. The HLR metric obtained with the PI controller also performed generally better (in the typical and worst scenarios), however, had similar results to the HLR metric obtained with the I controller in the critical scenario.

Table 6. System performance with PI controller for the cases analyzed in three turbulence profiles (T_1 , T_2 , and T_3) according to the metrics of FWHM [Pixel], HLR [Pixel], and Strehl ratio [%].

Metrics	Typical Scenario			Worst Scenario			Critical Scenario		
	T_1	T_2	T_3	T_1	T_2	T_3	T_1	T_2	T_3
FWHM	15.625	15.375	15.500	36.625	29.500	30.875	66.750	72.750	72.625
HLR	7.75	7.75	7.50	22.00	22.75	24.00	30.75	31.75	31.75
Strehl ratio	3.091%	3.552%	3.428%	0.494%	0.528%	0.396%	0.193%	0.182%	0.184%

4.2.4. Hybrid Fuzzy Proportional Integral Controller

The hybrid fuzzy PI controller was designed using the structure of Figure 1, a PI controller with a gain scheduler based on fuzzy logic. As an input for the gain scheduler, the RMS value of the residual and the total wavefront error were adopted. The primary justification for selecting these metrics as inputs in the fuzzy logic system lies in their facility to be computed in real-time systems.

For each scheduler input, three triangular membership functions were adopted, categorizing the inputs into the linguistic terms high, medium, and low, as pointed out in Figure 9a. The residual wavefront membership functions assume values within the range of [0, +0.5], and for the total wavefront membership functions the interval was designed within the range of [0.4, 1.2]. The gain scheduler has two outputs, referring to the proportional gain and integral time, in which membership functions were also fitted in triangular functions with the same linguistic terms.

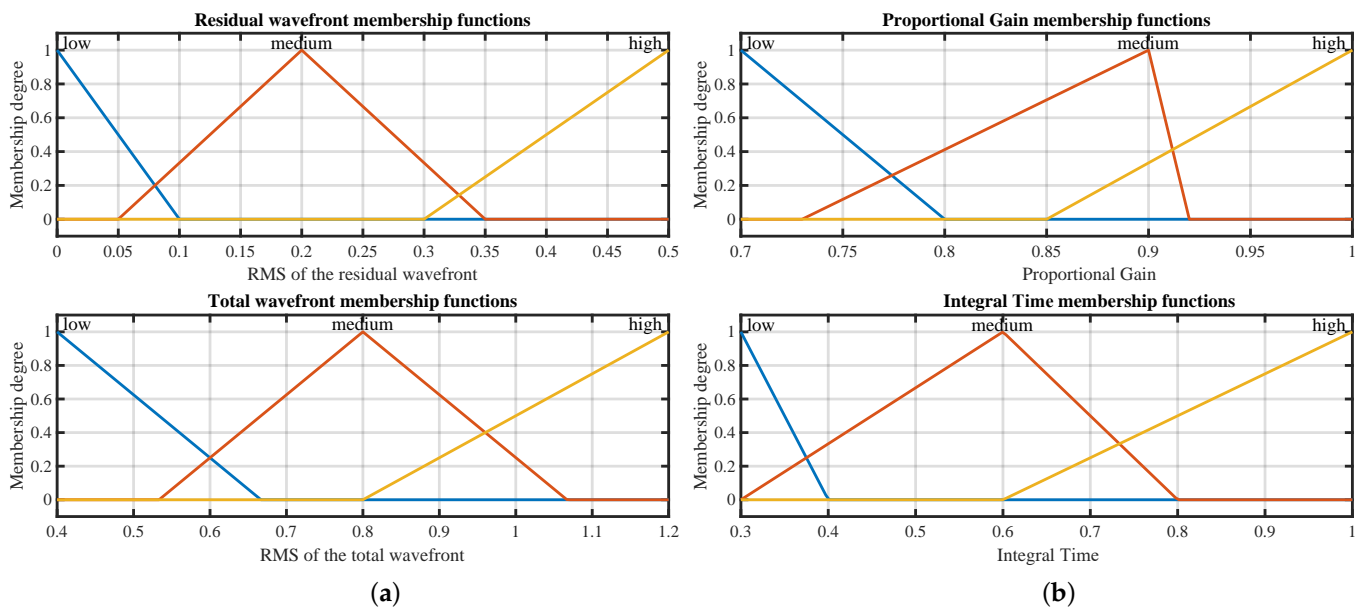


Figure 9. Triangular membership functions with the linguistic terms low, medium, and high for: (a) input variables (RMS value of the residual and total wavefront error), and (b) output variables (proportional gain and integral time).

Figure 9b depicts the membership functions for the proportional gain and integral time, respectively. Considering that traditional PID control tuning methods are not readily applicable to the proposed multi-input, multiple-output (MIMO), and non-linear system,

the PI parameters were empirically tested, adjusted, and fine-tuned to enhance the performance of the AO system, with a focus on improving the metrics of FWHM, HLR, and Strehl ratio. During the tests, the integral time was systematically adjusted within the range of 0.1 to 1, while the proportional action was varied between 0.5 and 5. The optimal parameters for the proportional-integral action controller are determined to be $K_p = 1$ and $T_i = 0.4$. Moreover, it has been observed that when the proportional gain values are set within the range of 0.7 to 1 and the integral time falls between 0.3 and 1, a stable condition is attained, resulting in effective AO control performance.

Figure 10a,b shows the fuzzy control surface that maps the given inputs (RMS values of the residual and total wavefront) to the outputs (i.e., the proportional and integral time). Lookup tables can be utilized to approximate the nonlinear control surfaces, resulting in simplified control code, and enhancing the execution speed. Furthermore, this approach facilitates the embedding of the designed fuzzy controller in real-time systems. In Figure 10a, there is a noticeable proportional gain scheduler, which is divided into three plateaus whereby the residual and total values remain in the middle ranges. The integral time schedule, conversely, presents a greater variation compared with the proportional gain schedule, with a minimum value being reached when the total effective values (i.e., RMS of the total wavefront) are around $0.7 \mu\text{m}$. Both outputs have their maximum values if the dominant membership function reaches the linguistic variable “high”.

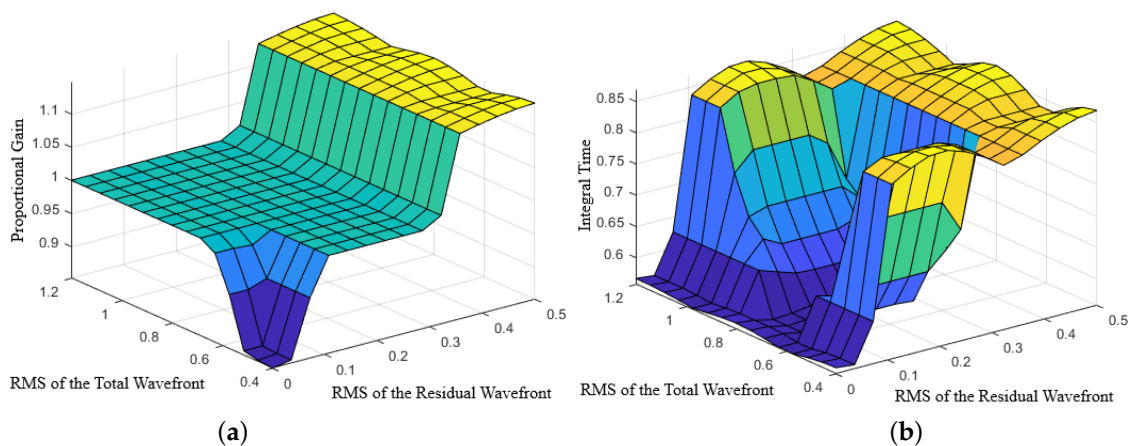


Figure 10. Fuzzy output surface (control surface plot) for: (a) proportional gain and (b) integral time.

Figure 11a–c corresponds to the PSFs of the first turbulence profile controlled by the fuzzy PI controller in the typical, worst, and critical scenarios, respectively. By comparing the surface plots of the typical case depicted in Figures 6–8 and 11, one can observe peak amplitudes (in counts) of about 5×10^7 (open loop), 4×10^8 (I controller), 10×10^8 (PI controller), and 15×10^8 (fuzzy PI controller), respectively. That is, in the fuzzy PI controller, the peak amplitude is found to be 30 times larger than that of the open-loop case, 3 times larger than the I controller, and 1.5 times larger than the PI controller. Comparing the PSFs of this control strategy with those presented by the PI controller, Figure 8, the fuzzy PI has a better overall performance. Additionally, it is noteworthy that the performance of the controllers, in all cases assessed, is significantly limited by the deterioration of the simulated atmospheric conditions. As can be seen in the performance of the critical case, that does not replicate the improvement observed in the typical case, even with the fuzzy PI controller.

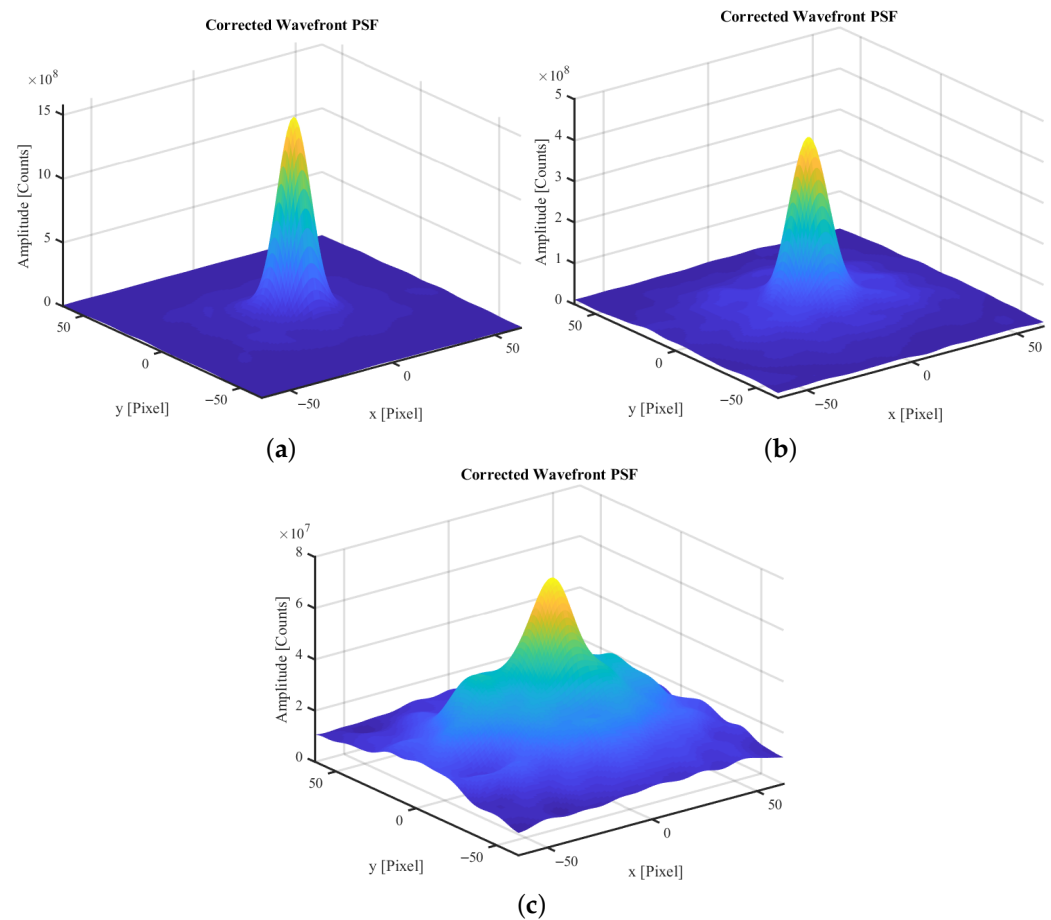


Figure 11. PSF of the first turbulence profile using fuzzy Proportional-Integral action controller for: (a) typical case, (b) worst case, and (c) critical case.

The metrics of FWHM, HLR, and Strehl ratio of this controller in all turbulence profiles are presented in Table 7.

Table 7. System performance with fuzzy PI controller for the cases analyzed in three turbulence profiles (T_1 , T_2 , and T_3) according to the metrics of FWHM [Pixel], HLR [Pixel], and Strehl ratio [%].

Metrics	Typical Scenario			Worst Scenario			Critical Scenario		
	T_1	T_2	T_3	T_1	T_2	T_3	T_1	T_2	T_3
FWHM	14.500	14.375	14.625	18.250	19.375	19.750	50.000	52.750	45.125
HLR	6.50	6.50	6.50	9.50	12.50	13.50	29.25	29.50	29.25
Strehl ratio	4.869%	5.112%	5.090%	1.377%	1.028%	0.844%	0.251%	0.240%	0.249%

4.2.5. Discussions

Figure 12a–c represents the wavefront RMS versus time of the open-loop system and closed-loop system under I, PI, and fuzzy PI controllers for all the turbulence profiles adopted. The fuzzy-based controller has a smaller RMS value in every single simulation and thus outperforms its peers. The open-loop simulations serve as a performance baseline for comparison, presenting greater values of wavefront RMS in the simulations. Between the classical controllers (I and PI algorithms), the results indicate that the PI version presents better results than the I controller.

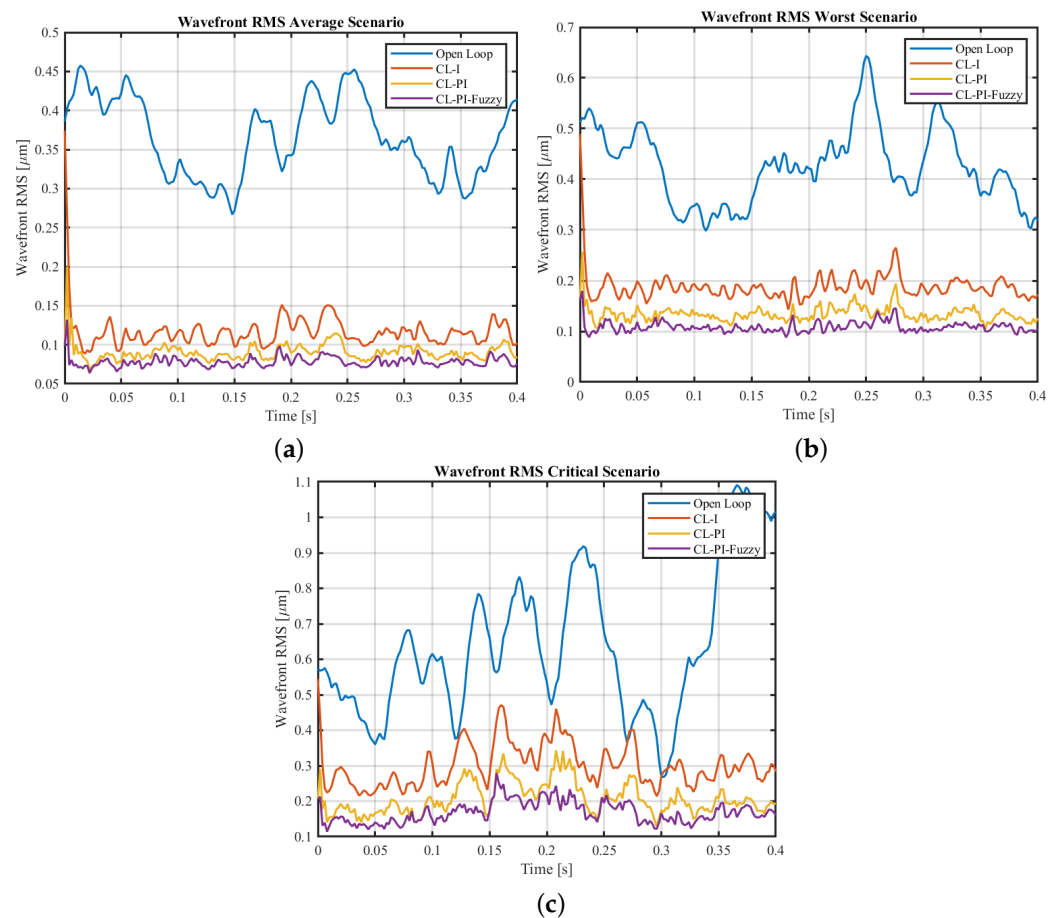


Figure 12. Wavefront RMS values over time for all the control strategies implemented: open loop, in a closed loop with I (CL-I), PI (CL-PI), and fuzzy PI (CL-PI-Fuzzy) controllers. Simulation scenarios: (a) typical case, (b) worst case, and (c) critical case.

Table 8 presents a summary of the mean and standard deviation values of the residual wavefront for the open-loop and closed-loop systems. The PI controller presents values consistently smaller than the I controller and open-loop system values. There is an improvement of about 75% to 80% in the mean value of the residual wavefront in the mean case while an improvement by about 70% occurs in the critical case. By analyzing the standard deviations of effective values of the wavefront, it is concluded that the PI controller has smaller deviations than the I action controller. However, it is observed that the standard deviations significantly grow with the worsening of atmospheric conditions, going from 0.008 μm in the first turbulence profile in the typical case to 0.045 μm in the first turbulence profile in the critical case. Based on the analysis conducted, it can be inferred that the I and PI controllers are insufficient for effectively controlling the system during critical scenarios.

The hybrid fuzzy PI controller, in turn, presents better results than the ones reported by the PI controller, with an improvement of about 80% when compared to the mean effective values of the wavefronts in open-loop in the typical case and about 75% compared to the critical case. In addition, the fuzzy PI strategy has a performance of about 10% better than the PI algorithm in the typical case and about 15% better in the critical scenario. This again reveals and reaffirms the potential of using intelligent controllers with dynamic gain scaling in AO systems.

Table 8. Performance of open loop systems (OL), in a closed loop with I controller (CL-I), with PI controller (CL-PI), with fuzzy PI controller (CL-PI-Fuzzy), for the scenarios analyzed in three turbulence profiles (T_1 , T_2 , and T_3) as a function of the metrics of the mean (RMS Mean) [μm] and the standard deviation of RMS values (RMS Std. Dev.) [μm].

Metrics	Controller	Typical Scenario			Worst Scenario			Critical Scenario		
		T_1	T_2	T_3	T_1	T_2	T_3	T_1	T_2	T_3
RMS Mean	OL	0.358	0.461	0.330	0.418	0.737	0.637	0.662	0.601	0.613
	CL-I	0.115	0.115	0.115	0.187	0.203	0.203	0.305	0.276	0.282
	CL-PI	0.090	0.088	0.087	0.134	0.151	0.148	0.212	0.190	0.195
	CL-PI-Fuzzy	0.078	0.079	0.077	0.108	0.125	0.125	0.172	0.161	0.163
RMS Std. Dev.	OL	0.049	0.104	0.075	0.076	0.232	0.197	0.213	0.123	0.101
	CL-I	0.013	0.017	0.016	0.018	0.030	0.026	0.057	0.031	0.043
	CL-PI	0.008	0.012	0.010	0.013	0.027	0.018	0.045	0.024	0.031
	CL-PI-Fuzzy	0.006	0.009	0.007	0.009	0.019	0.018	0.030	0.018	0.024

5. Conclusions

This work demonstrates the results of the integration of the OOMAO toolbox with Simulink. As proof of concept, we have evaluated AO control strategies based on I, PI, and hybrid PI fuzzy controllers, analyzing them using realistic atmospheric data in the context of the SOAR telescope. The hybrid fuzzy PI controller reported a 25% increase in the FWHM metrics in the critical scenario if compared with open-loop metrics in the critical case. The results highlight the limitations of classical control techniques when applied to AO systems. Moreover, the results of the hybrid fuzzy PI controller demonstrate the potential of intelligent control techniques to improve control performance in hostile atmospheric conditions, thus expanding the viability of AO applications in regions of high atmospheric turbulence. In that sense, fixed-gain controllers are limited in conditions of fast-changing scenarios, as presented by atmospheric turbulence. In these cases, adaptive strategies using gain scheduling and intelligent controllers might be more suitable as a control technique. Moreover, it is expected that the fuzzy PI controller retains their superior performance compared to classical approaches (I and PI controllers) in different scenarios (e.g., modification of the telescope and site) since the fuzzy strategy itself allows greater flexibility for tuning and control. Further tests to evaluate different scenarios will be conducted in future works.

Author Contributions: Conceptualization, V.C. and W.B.; methodology, V.C. and W.B.; software, V.C.; validation, V.C. and W.B.; formal analysis, V.C. and W.B.; investigation, V.C. and W.B.; resources, V.C. and W.B.; data curation, V.C. and W.B.; writing—original draft preparation, V.C. and W.B.; writing—review and editing, V.C. and W.B.; supervision, V.C. and W.B.; project administration, V.C. and W.B.; funding acquisition, W.B. All authors have read and agreed to the published version of the manuscript.

Funding: This study was financed in part by the Coordenação de Aperfeiçoamento de Pessoal de Nível Superior-Brasil (CAPES)-Finance Code 001. This research also received partial support from the Fundação de Amparo à Pesquisa do Estado de São Paulo (FAPESP) under Grants 2022/10909-5 and 2023/04428-7.

Institutional Review Board Statement: Not applicable.

Informed Consent Statement: Not applicable.

Data Availability Statement: The data presented in this study are available on request from the corresponding author.

Acknowledgments: The authors acknowledge the support of the Astronomy Instrumentation Group of the Institute of Astronomy, Geophysics and Atmospheric Sciences (IAG) of the University of São Paulo (USP).

Conflicts of Interest: The authors declare no conflict of interest.

References

1. Pullen, W.C.; Wang, T.; Choi, H.; Ke, X.; Negi, V.S.; Huang, L.; Idir, M.; Kim, D. Statistical Tool Size Study for Computer-Controlled Optical Surfacing. *Photonics* **2023**, *10*, 286. [[CrossRef](#)]
2. Hippler, S. Adaptive Optics for Extremely Large Telescopes. *J. Astron. Instrum.* **2019**, *8*, 1950001. [[CrossRef](#)]
3. Hardy, J.W. *Adaptive Optics for Astronomical Telescopes*; Oxford University Press: New York, NY, USA, 1998.
4. Tyson, R.K. *Topics in Adaptive Optics*; IntechOpen: Rijeka, Croatia, 2012. [[CrossRef](#)]
5. Davies, R.; Kasper, M. Adaptive Optics for Astronomy. *Annu. Rev. Astron. Astrophys.* **2012**, *50*, 305–351. [[CrossRef](#)]
6. Madec, P.Y. Overview of Deformable Mirror Technologies for Adaptive Optics and Astronomy. In Proceedings of the SPIE—The International Society for Optical Engineering, Amsterdam, The Netherlands, 2 June 2012; Volume 844705. [[CrossRef](#)]
7. Ellerbroek, B.L.; Vogel, C.R. Simulations of Closed-loop Wavefront Reconstruction for Multiconjugate Adaptive Optics on Giant Telescopes. In Proceedings of the Astronomical Adaptive Optics Systems and Applications, International Society for Optics and Photonics, SPIE, San Diego, CA, USA, 24 December 2003; Tyson, R.K., Lloyd-Hart, M., Eds.; Volume 5169, pp. 206–217. [[CrossRef](#)]
8. Faes, D.M.; Tokovinin, A.; Vieira, T.; Mello, A.; Domingues, M.; Andrade, D.; Quint, B.C.; dos Santos, J.B., Sr. SAMplus: Adaptive Optics at Optical Wavelengths for SOAR. In Proceedings of the Adaptive Optics Systems VI, International Society for Optics and Photonics, SPIE, Austin, TX, USA, 11 July 2018; Close, L.M., Schreiber, L., Schmidt, D., Eds.; Volume 10703, pp. 983–992. [[CrossRef](#)]
9. Basden, A.G.; Jenkins, D.; Morris, T.J.; Osborn, J.; Townson, M.J. Efficient Implementation of Pseudo Open-Loop Control for Adaptive Optics on Extremely Large Telescopes. *Mon. Not. R. Astron. Soc.* **2019**, *486*, 1774–1780. [[CrossRef](#)]
10. Gu, H.; Zhao, Z.; Zhang, Z.; Cao, S.; Wu, J.; Hu, L. High-Precision Wavefront Reconstruction from Shack-Hartmann Wavefront Sensor Data by a Deep Convolutional Neural Network. *Meas. Sci. Technol.* **2021**, *32*, 085101. [[CrossRef](#)]
11. Shatokhina, I.; Hutterer, V.; Ramlau, R. Review on Methods for Wavefront Reconstruction from Pyramid Wavefront Sensor Data. *J. Astron. Telesc. Instrum. Syst.* **2020**, *6*, 1–39. [[CrossRef](#)]
12. Bond, C.Z.; Hadi, K.E.; Sauvage, J.F.; Correia, C.; Fauvarque, O.; Rabaud, D.; Lamb, M.; Neichel, B.; Fusco, T. Experimental Study of an Optimised Pyramid Wave-front Sensor for Extremely Large Telescopes. In Proceedings of the Adaptive Optics Systems V, International Society for Optics and Photonics, SPIE, Edinburgh, UK, 27 July 2016; Marchetti, E., Close, L.M., Véran, J.P., Eds.; Volume 9909, pp. 1783–1795. [[CrossRef](#)]
13. Schatz, L.; Males, J.R.; Correia, C.M.; Neichel, B.; Chambouleyron, V.; Codona, J.L.; Fauvarque, O.; Sauvage, J.F.; Fusco, T.; Hart, M.; et al. Three-Sided Pyramid Wavefront Sensor, Part 1: Simulations and Analysis for Astronomical Adaptive Optics. *J. Astron. Telesc. Instrum. Syst.* **2021**, *7*, 1–19. [[CrossRef](#)]
14. Yang, H.; Jin, Y.; Hu, Y.; Zhang, D.; Yu, Y.; Liu, J.; Li, J.; Jiang, X.; Yu, X. Image Degradation Model for Dynamic Star Maps in Multiple Scenarios. *Photonics* **2022**, *9*, 673. [[CrossRef](#)]
15. Folcher, J.P.; Carbillet, M.; Ferrari, A.; Abelli, A. Adaptive Optics Feedback Control. *Eur. Astron. Soc. Publ. Ser.* **2013**, *59*, 93–130. [[CrossRef](#)]
16. Rigaut, F.; Van Dam, M. Simulating Astronomical Adaptive Optics Systems Using Yao. In Proceedings of the Third AO4ELT Conference, Florence, Italy, 26–31 May 2013; Esposito, S., Fini, L., Eds.; p. 18. [[CrossRef](#)]
17. Reeves, A. Soapy: An Adaptive Optics Simulation Written Purely in Python for Rapid Concept Development. In Proceedings of the Adaptive Optics Systems V, International Society for Optics and Photonics, SPIE, Edinburgh, UK, 27 July 2016; Marchetti, E., Close, L.M., Véran, J.P., Eds.; Volume 9909, pp. 2173–2183. [[CrossRef](#)]
18. Townson, M.J.; Farley, O.J.D.; de Xivry, G.O.; Osborn, J.; Reeves, A.P. AOtools: A Python Package for Adaptive Optics Modelling and Analysis. *Opt. Express* **2019**, *27*, 31316–31329. [[CrossRef](#)] [[PubMed](#)]
19. Conan, R.; Correia, C. Object-oriented Matlab Adaptive Optics Toolbox. In Proceedings of the Adaptive Optics Systems IV, International Society for Optics and Photonics, SPIE, Montréal, QC, Canada, 7 August 2014; Marchetti, E., Close, L.M., Véran, J.P., Eds.; Volume 9148, pp. 2066–2082. [[CrossRef](#)]
20. Assémat, F.; Wilson, R.W.; Gendron, E. Method for Simulating Infinitely Long and Non Stationary Phase Screens with Optimized Memory Storage. *Opt. Express* **2006**, *14*, 988–999. [[CrossRef](#)]
21. Nousiainen, J.; Rajani, C.; Kasper, M.; Helin, T. Adaptive Optics Control Using Model-Based Reinforcement Learning. *Opt. Express* **2021**, *29*, 15327–15344. [[CrossRef](#)] [[PubMed](#)]
22. Ogata, K. *Modern Control Engineering*, 5th ed.; Prentice Hall: Upper Saddle River, NJ, USA, 2009.
23. Åström, K.J.; Wittenmark, B. *Computer-Controlled Systems—Theory and Design*; Prentice-Hall, Inc.: Upper Saddle River, NJ, USA, 1997.
24. AlSabbah, S.; AlDhaifallah, M.; Al-Jarrah, M. Design of Multiregional Supervisory Fuzzy PID Control of pH Reactors. *J. Control Sci. Eng.* **2015**, *2015*, 396879. [[CrossRef](#)]
25. Ke, X.; Zhang, D. Fuzzy Control Algorithm for Adaptive Optical Systems. *Appl. Opt.* **2019**, *58*, 9967–9975. [[CrossRef](#)] [[PubMed](#)]
26. Flores-Meza, R.; Sotelo, P.D.; Garfias, F.; Cuevas, S.; Sanchez, L.J. Adaptive Optics Tip-Tilt System with Fuzzy Control. In Proceedings of the Adaptive Optical Systems Technology, International Society for Optics and Photonics, SPIE, Munich, Germany, 7 July 2000; Wizinowich, P.L., Ed.; Volume 4007, pp. 671–681. [[CrossRef](#)]
27. Nousiainen, J.; Rajani, C.; Kasper, M.; Helin, T.; Haffert, S.Y.; Vérinaud, C.; Males, J.R.; Van Gorkom, K.; Close, L.M.; Long, J.D.; et al. Toward On-Sky Adaptive Optics Control Using Reinforcement Learning—Model-based Policy Optimization for Adaptive Optics. *A&A* **2022**, *664*, A71. [[CrossRef](#)]

28. Pou, B.; Ferreira, F.; Quinones, E.; Gratadour, D.; Martin, M. Adaptive Optics Control with Multi-Agent Model-Free Reinforcement Learning. *Opt. Express* **2022**, *30*, 2991–3015. [[CrossRef](#)] [[PubMed](#)]
29. Guo, Y.; Zhong, L.; Min, L.; Wang, J.; Wu, Y.; Chen, K.; Wei, K.; Rao, C. Adaptive Optics Based on Machine Learning: A Review. *Opto-Electron. Adv.* **2022**, *5*, 200082-1–200082-20. [[CrossRef](#)]
30. Conan, R.; Bennet, F.; Bouchez, A.H.; van Dam, M.A.; Espeland, B.; Gardhouse, W.; d’Orgeville, C.; Parcell, S.; Piatrou, P.; Price, I.; et al. The Giant Magellan Telescope Laser Tomography Adaptive Optics System. In Proceedings of the Adaptive Optics Systems III, International Society for Optics and Photonics, SPIE, Amsterdam, The Netherlands, 13 September 2012; Ellerbroek, B.L., Marchetti, E., Véran, J.P., Eds.; Volume 8447, pp. 1271–1287. [[CrossRef](#)]
31. Andersen, D.; Stoesz, J.; Morris, S.; Lloyd-Hart, M.; Crampton, D.; Butterley, T.; Ellerbroek, B.; Jolissaint, L.; Milton, N.M.; Myers, R.; et al. Performance Modeling of a Wide-Field Ground-Layer Adaptive Optics System. *Publ. Astron. Soc. Pac.* **2006**, *118*, 1574–1590. [[CrossRef](#)]

Disclaimer/Publisher’s Note: The statements, opinions and data contained in all publications are solely those of the individual author(s) and contributor(s) and not of MDPI and/or the editor(s). MDPI and/or the editor(s) disclaim responsibility for any injury to people or property resulting from any ideas, methods, instructions or products referred to in the content.